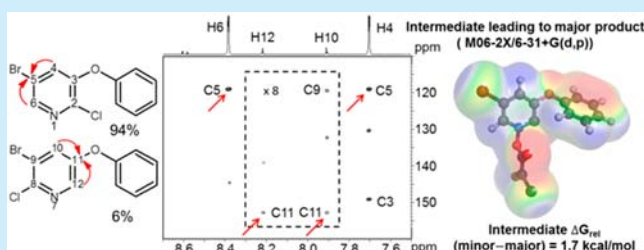


Application of 1,1-ADEQUATE, HMBC, and Density Functional Theory To Determine Regioselectivity in the Halogenation of Pyridine N-Oxides

Tsang-Lin Hwang*,[†] Michael D. Bartberger*,[‡] and Ying Chen[§][†]Attribute Sciences, [‡]Molecular Engineering, Therapeutic Discovery, and [§]Drug Substance Technologies, Amgen, Inc., One Amgen Center Drive, Thousand Oaks, California 91320, United States

Supporting Information

ABSTRACT: The 1,1-ADEQUATE spectrum clearly shows specific two-bond proton to carbon correlations to unequivocally distinguish the major and minor regioisomers of ortho-halogenated pyridines and to aid in assignment of the corresponding proton and carbon chemical shifts. M06-2X/6-31+G(d,p) free energies of the regioisomeric intermediates arising from deprotonation correctly predict the experimentally observed preference and thus can be used to tune the substituent pattern to yield a desired regiochemical outcome.



Structural elucidation of regioisomers often relies on mass spectrometry data for molecular formula and on 1D and 2D NMR data to establish and distinguish the regioisomeric structures. Among the array of 2D NMR techniques, the heteronuclear multiple bond correlation (HMBC)¹ experiment was designed to utilize $^nJ_{CH}$ couplings to correlate long-range proton to carbon connectivities for the structural elucidation of molecules. These correlations are crucial to assign the chemical shifts of quaternary carbons and connect different moieties of a molecule together in order to determine the molecular skeleton. Although the HMBC experimental data usually contain two- and three-bond proton to carbon correlations, longer four- and five-bond correlations can also appear. Because the number of bonds in these correlations is not specific in the HMBC data, the data may fit into several possible structures or may result in ambiguous chemical shift assignments. To resolve these ambiguities, carrying out further experiments to distinguish two- and three-bond correlations is necessary. Experiments designed for this purpose include $^2J_{CH}$ HMBC,² H2BC,³ and 1,1-ADEQUATE.^{4,5} In essence, $^2J_{CH}$ HMBC uses $^3J_{HH}$, $^2J_{CH}$, and $^3J_{CH}$ couplings, while H2BC applies $^1J_{CH}$ and $^nJ_{HH}$ couplings to differentiate two- or three-bond correlations between proton and proton-bearing carbons. 1,1-ADEQUATE employs $^1J_{CC}$ coupling to generate two-bond correlations between proton and carbon and extends the correlation to quaternary carbon. The specific two-bond proton to carbon correlation from 1,1-ADEQUATE can speed up the determination of the correct structure using the computer-assisted structure elucidation (CASE) algorithm.⁶ Other examples using 1,1-ADEQUATE for unambiguous structure elucidation include (1) determination of the substitution site on the pyrrole moiety of natural products (Figure 1a,b),⁷ where the 3-pyrrolyl derivative was elucidated as the 2-pyrrolyl derivative previously,⁸ and (2) structural revision of coniothyronine with

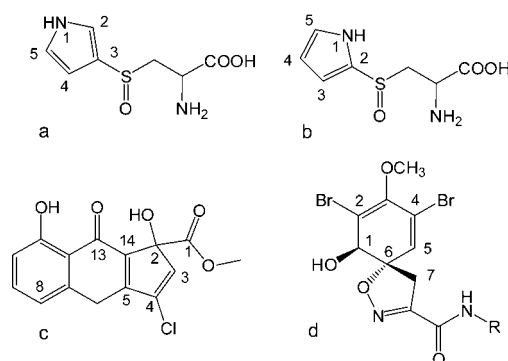


Figure 1. Structures for the substituted pyrrole compounds (a, b), coniothyronine (c), and bromotyrosine-derived metabolite (d).

respect to the Cl position attached to C4 instead of C3 (Figure 1c).^{9,10} Additional structural elucidation examples using the ADEQUATE family of experiments have recently been reviewed.¹¹

In addition to the possibility of incorrect structure elucidation of regioisomers without two-bond proton-to-carbon connectivity information, misassignment of quaternary carbon chemical shifts can also occur. Kalaitzis et al. surveyed the literature and found that the ^{13}C assignments of two brominated carbons C2 and C4 in the cyclohexadienyl ring moiety of bromotyrosine-derived metabolites (Figure 1d) were misassigned in more than 20 compounds.¹² These errors were mainly due to utilization of earlier data without further verification. For the correct assignment of these quaternary carbon chemical shifts, the authors show that in the HMBC

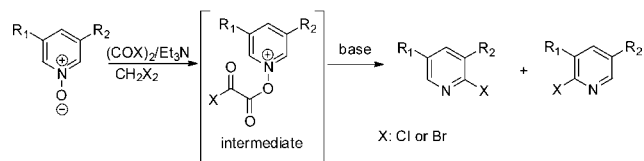
Received: February 4, 2016

Published: April 7, 2016

spectrum of such metabolite, derived from marine sponges, the unambiguous assignment of C2 at 112–113 ppm comes from the correlation of 1-OH to C2 in the cyclohexadienyl ring, which resolves the ambiguity that both H1 and H5 in the cyclohexadienyl ring correlate to C2 and C4 in the HMBC data. Ambiguities such as that described above can be also resolved by 1,1-ADEQUATE in a few hours using NMR equipped with a cryoprobe setup, allowing for structural determination of natural products requiring only a few milligrams of isolated material.⁶

During the course of development of a drug candidate for an internal clinical program, we became interested in a highly regioselective halogenation reaction (Scheme 1; X = Cl/Br)

Scheme 1. Highly Regioselective Halogenation Addition to 3,5-Disubstituted Pyridine Derivatives^{1,4}



involving addition to 3,5-disubstituted pyridine derivatives at either the C2 or C6 position.¹³ Given the two possible regiochemical outcomes, unequivocal characterization (and, ultimately, control) of regioselectivity was critically important.

Similar to the ambiguous ¹³C assignment issue in the cyclohexadienyl ring examples mentioned above, the protons at position 2 or 6 in both regioisomeric products from Scheme 1 have correlations to C3 and C5 in the HMBC data. In this study, we report the application of 1,1-ADEQUATE and HMBC to clearly distinguish C2 and C6 regioisomers in mixtures obtained from the halogenation reaction above and the use of density functional theory to calculate the difference of Gibbs free energy between regioisomeric intermediates to correctly predict the major and minor products.

Figure 2a shows the chlorination reaction with 2-bromo-4-phenoxy pyridine *N*-oxide **1**. The major and minor chlorinated regioisomers **2** and **3** in the sample have H6 and H12 proton peaks at 8.40 and 8.22 ppm, respectively, in a ratio of about 94 to 6. In the HMBC spectrum (Figure 2b), H6 has correlations to C5 at 119.1 ppm and C3 at 144.7 ppm, while H12 has correlations to C9 at 119.4 ppm and C11 at 152.9 ppm. Although C5 and C9 (and C3 and C11) have similar carbon chemical shifts, the intensity of the H6 to C5 correlation peak is stronger than that of the H6 to C3 peak, indicating that H6 to C5 is a two-bond proton to carbon correlation, while H6 to C3 is a four-bond correlation. Similarly, H12 to C11 has a stronger correlation peak intensity than that of H12 to C9, indicating that H12 to C11 is a two-bond correlation. Measurement of long-range proton-to-carbon coupling constants by HSQMB-type experiments¹⁵ shows that ²*J*_{H6,C5} and ⁴*J*_{H6,C3} of **2** are 5.5 and 1.9 Hz, respectively, and ²*J*_{H12,C11} and ⁴*J*_{H12,C9} of **3** are 3.7 and 1.9 Hz, respectively (see the Supporting Information). This observation is consistent with the peak intensities in the HMBC spectrum. The corroborating 1,1-ADEQUATE spectrum of the mixture of **2** and **3** in Figure 2c shows H6 and H4 have two-bond correlations to C5, while H10 and H12 have two-bond correlations to C11. Since H4 and H10 are in the para position to the pyridyl nitrogen, additional two-bond correlations are observed for H4 to C3 and H10 to C9, respectively. These data confirm that the major regioisomer possesses the Cl substituent

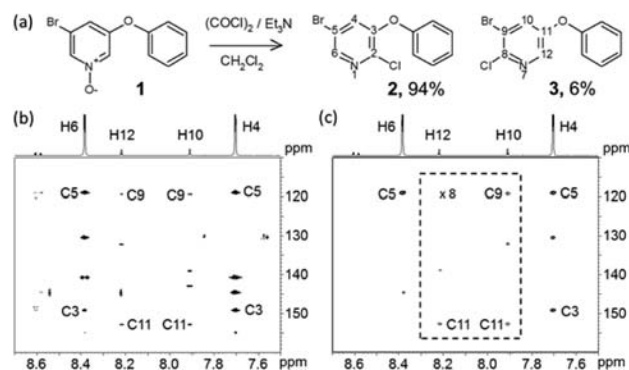


Figure 2. Comparison of HMBC and 1,1-ADEQUATE spectra of the mixture of compounds **2** and **3**. The sample was 80 mg/mL in DMSO-*d*₆. For constant-time HMBC,¹⁶ long-range *J*_{CH} was set to 8 Hz, spectral width in *F*₂ = 2.4 ppm, transmitter centered at 7.8 ppm with 2048 data points acquisition, and for 1,1-ADEQUATE (adeq11etgprdsp in the Bruker library), *J*_{CH} was set to 160 Hz, *J*_{CC} = 60 Hz, spectral width in *F*₂ = 10 ppm, transmitter centered at 5 ppm with 2048 data points acquisition and ¹³C decoupling during acquisition. For both HMBC and 1,1-ADEQUATE, *d*₁ = 1 s, and spectral width in *F*₁ = 70 ppm where transmitter centered at 135 ppm. For HMBC, number of increments in *F*₁ = 256 with 16 scans per increment, and for 1,1-ADEQUATE, number of increments in *F*₁ = 128 increments with 256 scans per increment. HMBC and 1,1-ADEQUATE took 2.2 and 11.1 h to acquire, respectively. Squared Sinebell window function was applied before Fourier transform of 2D data. In the *F*₁ dimension, the data points were forward linear predicted to 1024 points. Magnitude mode display was used in the *F*₂ dimension for HMBC data.

attached at the 2 position, while the minor regioisomer incorporates Cl at the 8 position.

Interestingly, when the reactant substituent was changed from phenoxy (**1**) to the phenylthio moiety (**4**) on the pyridine *N*-oxide ring, the minor and major chlorinated regioisomers **5** and **6** possess a ratio of ~22 to 78 (Figure 3a), opposite the result for the reaction in Figure 2a.

In the HMBC spectrum of the mixture of compounds **5** and **6** (Figure 3b), H6 at 8.39 ppm has a stronger correlation to C5 at 119.4 ppm (²*J*_{H6,C5} = 5.1 Hz) and a weaker correlation to C3 at 136.7 ppm (⁴*J*_{H6,C3} = 1.7 Hz), while H12 at 8.30 ppm has a weaker correlation to C9 at 119.8 ppm (⁴*J*_{H12,C9} = 1.8 Hz) and a

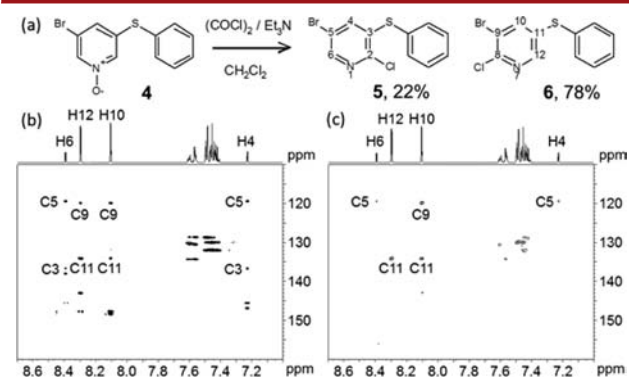
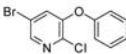
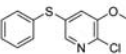
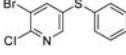
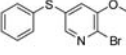
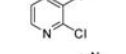
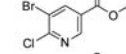
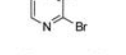
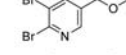
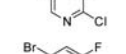
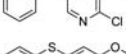
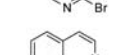
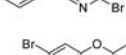
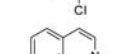
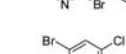
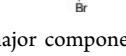



Figure 3. Comparison of HMBC and 1,1-ADEQUATE spectra of the mixture of compounds **5** and **6**. The sample was about 5.5 mg/mL in DMSO-*d*₆. Experimental parameters were the same as those in Figure 2. The weakest H6 to C5 correlation peak is above the noise level, and the corresponding 1D slice taken at the carbon frequency 119.4 ppm shows the peak has an S/N ratio of ~2.6.

stronger correlation to C11 at 134.1 ppm ($^2J_{\text{H12,C11}} = 6.8$ Hz). The unambiguous 1,1-ADEQUATE spectrum (Figure 3c) shows H6 and H4 have two-bond correlations to C5, while H10 and H12 have two-bond correlations to C11. These data confirm that the major component has Cl attached at the 8 position and the minor component has Cl at the 2 position.

After establishing the capability of this methodology to distinguish the regioisomers in the reaction samples, we acquired 1D and 2D NMR data for structure elucidation of the synthesized compounds listed in Table 1. For compounds

Table 1. Regioisomer Ratios for Different Substituents Used for Scheme 1 Reaction^a

entry	major product	regioselectivity	entry	major product	regioselectivity
2		93.6:6.4	13		100:0
6		77.9:22.1	14		98.4:1.6
7		100:0	15		99.4:0.6
8		100:0	16		98.8:1.2
9		100:0	17		98.3:1.7
10		100:0	18		82.9:17.1
11		100:0	19		93.7:6.3
12		100:0	20		73.5:26.5

^aThe major components are shown.

7–12, proton coupling constants are sufficient to distinguish the location of Cl or Br incorporation. For other compounds, HMBC and 1,1-ADEQUATE data were used to confirm the structure of the major regioisomer. For the minor component, we then looked into the 1D aromatic region for doublet peaks originating from the ortho proton next to nitrogen in the pyridyl moiety. The doublet peak from the minor component at a low level (~1–2%) may not have sufficient S/N for correlation peaks in 1,1-ADEQUATE due to the small amount of material. Nevertheless, in HMBC, the correlation peaks for minor components in all samples show up clearly. If the correlation patterns and corresponding carbon chemical shifts from the minor doublet peak are similar to those from the major regioisomer, the minor component can be classified as a regioisomer of the major component. Otherwise, the doublet peak from the minor component is from an impurity in the sample. For example, in compounds 13 and 17 in Table 1, small doublet peaks from impurities, at 1.2 and 0.8% levels relative to 13 and 17, respectively, have correlations to bromine-bearing carbon around 118 ppm, instead of ~134 ppm for the phenylthio-substituted carbon.

Given the sometimes significant changes in regiochemical preference upon differing substitution at one of the meta positions of the pyridyl ring (e.g., reversal in the cases of systems 9 and 10 versus 15 and 16 and systems 2 and 19 versus 6), it was of interest to determine whether the regiochemical

outcome of the halogen-capture step could be predicted in a straightforward manner using computational techniques, utilizing the relative energetics of the putative intermediates involved in the reaction. Density functional theory calculations¹⁷ at the M06-2X/6-31+G(d,p) level¹⁸ were used to characterize the (net charge neutral) intermediates arising from the proposed Et₃N-mediated deprotonation of the *O*-oxalylated *N*-oxide substrate. Figure 4 depicts the relevant structural parameters,

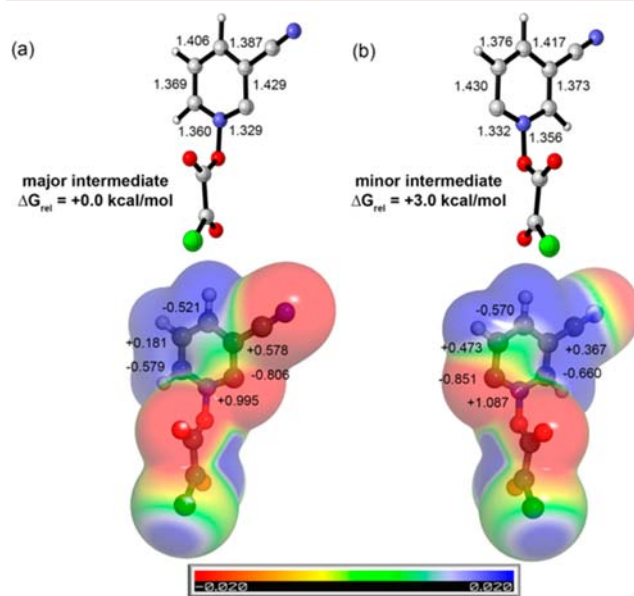


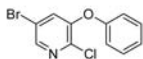
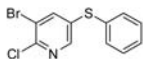
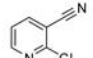
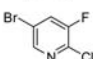
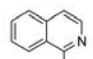
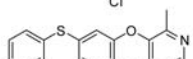
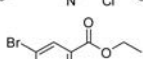
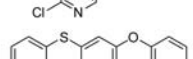
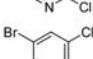
Figure 4. Ring interatomic distances (top) and electrostatic potential mapped onto the total electron density (0.001 au contour level; bottom) for 7, with resultant atomic charges for the major and minor deprotonated intermediates depicted in Scheme 1 based on M06-2X/6-31+G(d,p).

ESP-derived atomic partial charges,¹⁹ and free energy differences between the putative intermediates of system 7 involved in halide capture.

While a previously proposed mechanism entailed electrophilic capture of halide by the above intermediate(s), structural and charge characteristics consistent with a pyridinium-2-ylide-type structure²⁰ are also readily evident. Indeed, a slight decrease in N1–C2 and N1–C6 bond lengths from ca. 1.34 Å in the *O*-oxalylated pyridinium precursor (not shown)²¹ to ca. 1.33 Å occurs upon deprotonation of the respective centers of the major and minor intermediates. This is accompanied by a high degree of charge separation between the pyridinium nitrogen and deprotonated carbon centers, each of which consistent with an ylide-like resonance structure.²²

Table 2 below provides a summary of the experimentally determined regioisomeric ratios and computed relative stabilities of both the major and minor deprotonation intermediates, as well as those of the final halogenated products. It is observed that, for all cases, the trend of regioisomeric ratio can be predicted from the energy differences of the corresponding deprotonated intermediates prior to halogenation, including the decreased regioselectivity for systems 6 and 20.²⁴ On the other hand, relative product stabilities are a poorer indicator of selectivity, not only for moderately selective systems 6 and 20, but also highly regioselective system 7.

Table 2. Product Ratios and Relative Free Energies of Intermediates and Final Halogenation Products

entry	major product	regioselectivity	ΔG_{rel} (minor-major); intermediate (kcal/mol) ^{a,b}	ΔG_{rel} (minor-major); final product (kcal/mol) ^{a,b}
2		93.6:6.4	+1.7	+0.4
6		77.9:22.1	+1.0	-0.3
7		100:0	+3.0	-1.4
9		100:0	+3.4	0.0
11		100:0	+8.2	+0.7
13		100:0	+2.9	+0.3
15		99.4:0.6	+3.7	+4.6
17		98.3:1.7	+1.9	+0.4
20		73.5:26.5	+0.2	-0.7

^aFrom the M06-2X/6-31G+(d,p) conformer possessing lowest Gibbs free energy at 298 K. ^bPositive values indicate greater stability of the intermediate or final product corresponding to that found experimentally.

In conclusion, we have shown the application of 1,1-ADEQUATE and HMBC for unequivocal structural elucidation of halogenation products of 3,5-disubstituted pyridine derivatives and their regioselectivity is determined by integration of corresponding peaks from different regioisomers in the 1D proton spectrum. When ambiguity for structural elucidation or chemical shift assignment occurs for similar systems, 1,1-ADEQUATE can be employed to resolve the uncertainty. For reactions of this type, the dominant regioisomer can be predicted from the relative stabilities of the deprotonated intermediates involved in the subsequent halogenation step. This allows for the computational investigation of optimal substituent pattern, prior to synthesis, in order to effect or maximize a desired regiochemical outcome.

■ ASSOCIATED CONTENT

Supporting Information

The Supporting Information is available free of charge on the ACS Publications website at DOI: 10.1021/acs.orglett.6b00370.

Proton to carbon long-range coupling constants for compounds 2, 3, 5, and 6, NMR chemical shift assignments and 1,1-ADEQUATE spectra for pyridyl rings of compounds in Table 1, Cartesian coordinates and energies computed for systems in Table 2, along with electrostatic potential-derived charges for O-oxalylated pyridinium N-oxide 7 and corresponding deprotonated intermediates (PDF)

■ AUTHOR INFORMATION

Corresponding Authors

*E-mail: thwang@amgen.com.

*E-mail: mbartber@amgen.com.

Notes

The authors declare no competing financial interest.

■ ACKNOWLEDGMENTS

The authors thank Dr. Jason Tedrow at Amgen, Inc., for helpful discussions.

■ REFERENCES

- Bax, A.; Summers, M. F. *J. Am. Chem. Soc.* **1986**, *108*, 2093.
- Krishnamurthy, V. V.; Russell, D. J.; Hadden, C. E.; Martin, G. E. *J. Magn. Reson.* **2000**, *146*, 232.
- Nyberg, N. T.; Duus, J. Ø.; Sørensen, O. W. *J. Am. Chem. Soc.* **2005**, *127*, 6154.
- Reif, B.; Köck, M.; Kerssebaum, R.; Kang, H.; Fenical, W.; Griesinger, C. *J. Magn. Reson., Ser. A* **1996**, *118*, 282.
- Köck, M.; Reif, B.; Fenical, W.; Griesinger, C. *Tetrahedron Lett.* **1996**, *37*, 363.
- Cheatham, S. F.; Kline, M.; Sasaki, R. R.; Blinov, K. A.; Elyashberg, M. E.; Molodtsov, S. G. *Magn. Reson. Chem.* **2010**, *48*, 571.
- Schraml, J.; Kubec, R.; Kučerová, P. *Magn. Reson. Chem.* **2011**, *49*, 147.
- Kučerová, P.; Kubec, R.; Šimek, P.; Václavík, L.; Schraml, J. *J. Agric. Food Chem.* **2011**, *59*, 1821.
- Martin, G. E.; Buevich, A. V.; Reibarkh, M.; Singh, S. B.; Ondeyka, J. G.; Williamson, R. T. *Magn. Reson. Chem.* **2013**, *51*, 383.
- Kong, F.; Zhu, T.; Pan, W.; Tsao, R.; Pagano, T. G.; Nguyen, B.; Marquez, B. *Magn. Reson. Chem.* **2012**, *50*, 829.
- Martin, G. E. In *Annual Reports on NMR Spectroscopy*; Webb, G. A., Ed.; Elsevier Ltd., 2011; Vol. 74, p 215.
- Kalaitzis, J. A.; Davis, R. A.; Quinn, R. J. *Magn. Reson. Chem.* **2012**, *50*, 749.
- Chen, Y.; Huang, J.; Hwang, T.-L.; Chen, M. J.; Tedrow, J. S.; Farrell, R. P.; Bio, M. M.; Cui, S. *Org. Lett.* **2015**, *17*, 2948.
- The proposed intermediate was not isolated.
- (a) Sauri, J.; Parella, T.; Espinosa, J. F. *Org. Biomol. Chem.* **2013**, *11*, 4473. (b) Sauri, J.; Espinosa, J. F.; Parella, T. *Angew. Chem., Int. Ed.* **2012**, *51*, 3919.
- Furrer, J. *Chem. Commun.* **2010**, *46*, 3396.
- Gaussian 09, Revision D.01. See the Supporting Information for the complete reference.
- Zhao, Y.; Truhlar, D. G. *Theor. Chem. Acc.* **2008**, *120*, 215.
- Singh, U. C.; Kollman, P. A. *J. Comput. Chem.* **1984**, *5*, 129.
- Liebman, J. F.; Simons, J. In *Molecular Structure and Energetics*; Liebman, J. F., Greenberg, A., Eds.; VCH, 1986; Vol. 1, p 51.
- See the Supporting Information for geometric parameters of all species investigated computationally in this paper, along with the electrostatic potential derived charges for the N-oxalylated pyridium form of 7 and resultant major and minor deprotonated intermediates.
- Indeed, an increase in positive charge at N1 (from ca. +0.5 to +1.0) is predicted upon deprotonation at either C2 or C6 of the O-oxalylated pyridinium of 7 using either the Merz–Kollman–Singh¹⁹- or CHELPG²³ ESP-based fitting schemes and the M06-2X/6-31+G(d,p) density.²¹
- Breneman, C. M.; Wiberg, K. B. *J. Comput. Chem.* **1990**, *11*, 361.
- Investigation of the relative stabilities of the intermediates corresponding to the species in Table 2, using an implicit (IEFPCM)²⁵ dichloromethane solvent model, does not change the predicted regiochemical preference. See the Supporting Information.
- Tomasi, J.; Mennucci, B.; Cammi, R. *Chem. Rev.* **2005**, *105*, 2999.